



# An investigation into pore structure fractal characteristics in tight oil reservoirs: a case study of the Triassic tight sandstone with ultra-low permeability in the Ordos Basin, China

Junjie Wang<sup>1,2,3</sup> · Shenghe Wu<sup>1,2</sup> · Qing Li<sup>1,2</sup> · Qiheng Guo<sup>4</sup>

Received: 13 May 2020 / Accepted: 2 September 2020 / Published online: 15 September 2020  
© Saudi Society for Geosciences 2020

## Abstract

Pore structure, which not only determines the microscopic characteristics of reservoirs but also controls the macroscopic physical properties of reservoirs, has been difficult to study in reservoir research. Fractal theory is an effective method for quantitative analysis of the irregular and complex pore structures of rocks. On the basis of high-pressure mercury intrusion experiments, the fractal dimensions of tight sandstones in the Yanchang Formation of the Triassic in the Ordos Basin are calculated by two methods (the water saturation method and mercury saturation method), and the fractal characteristics of the pore structures in this tight sandstone reservoir are also analyzed. The results show that the pore structures of tight sandstone reservoirs are heterogeneous and can be divided into four types. The fractal dimensions calculated by the water saturation method are poorly correlated with reservoir quality, while the fractal dimensions calculated by the mercury saturation method have good correlation with reservoir quality, that is, reservoirs with low fractal dimensions have high reservoir permeability and large pore-throat radii, while reservoirs with high fractal dimensions have low reservoir permeability and small pore-throat radii. Therefore, the fractal dimensions calculated by the mercury saturation method are presented to characterize tight sandstone reservoirs. The pore structures with large pore-throat sizes (radius  $> r_{tr}$ ) and small pore-throat sizes (radius  $< r_{tr}$ ) are relatively independent, and this results in clear turning points on the fractal curves of most samples. More importantly, samples with different fractal characteristics can represent reservoirs with different physical properties and pore structures. In conclusion, fractal dimensions can be used as an effective parameter for the quantitative characterization of tight sandstone reservoir with ultra-low permeability.

**Keywords** Tight sandstone reservoir · Pore structure · Fractal dimension · Fractal characteristics · Ordos Basin

## Introduction

Tight oil reservoir is defined as oil-bearing rocks with porosity lower than 10% and air permeability lower than 1 mD in

China (Zou et al. 2012), and has become a significant unconventional resource in recent years (Zhu et al. 2008). For tight reservoirs, the pore structure not only controls the seepage characteristics of reservoir but also directly affects the production and ultimate recovery of tight oil well (Bustin et al. 2008; Ross and Bustin 2009; Camp 2011; Yang et al. 2013; Wu et al. 2013; Zhu et al. 2016; Gao et al. 2011). Compared to conventional sandstone reservoir, tight sandstone reservoir is difficult to characterize due to the narrow pore-throat size distributions, complex and strong heterogeneity pore structures (Li et al. 2018a, b). Therefore, quantitative evaluation of the pore structures in tight sandstone reservoir, especially the characterization of irregular pore shapes and complex pore-throat connectivity, has become the most challenging work in pore structure research.

The fractal geometry theory founded by Mandelbrot (1977) provides new ideas and methods for explaining various complex and irregular natural phenomena and for solving related

---

Responsible Editor: Santanu Banerjee

---

✉ Junjie Wang  
690732461@qq.com

<sup>1</sup> College of Geosciences, China University of Petroleum, Beijing 102249, China

<sup>2</sup> State Key Laboratory of Petroleum Resource and Prospecting, Beijing 102249, China

<sup>3</sup> Present address: China University of Petroleum-Beijing, 18 Fuxue Road, Changping, Beijing 102249, China

<sup>4</sup> Exploration and Development Research Institute of PetroChina Changqing Oilfield Company, Xi'an 710018, China

problems (Mandelbrot and Wheeler 1983; Wang et al. 2015; Ji et al. 2016). This theory is a powerful tool for studying complex systems with fractal characteristics in nature (Avnir et al. 1984). Pfeifer and Avnir (1983) were the first to verify the fractal structure of pores in reservoirs with a molecular adsorption method. At present, the fractal theory has been widely used in the field of petroleum exploration and development, especially in the study of reservoir pore structures (Katz and Thompson 1985; Krohn 1988; Xie et al. 2010; Jouini et al. 2011; Hu et al. 2012), and it has become a simple and effective way to quantitatively characterize the complexity and heterogeneity of reservoir pore structures. The fractal dimension  $D_f$  is an important parameter for characterizing fractal objects and has been widely used in quantitatively describing the complexity of reservoir pore structures. There are many methods for calculating the fractal dimension, including casting thin sections, mercury intrusion experiments, and nitrogen adsorption experiment (Thompson et al. 1987; Wang et al. 2013). Although previous studies have suggested that fractal theory is applicable to conventional reservoirs, there is still some controversy about whether the fractal theory can be applied to tight sandstone reservoirs and how to characterize pore structures in tight sandstone reservoir by fractal dimension.

The Upper Triassic Yanchang Formation of the Huaqing area in the Ordos Basin is an important tight oil reservoir with permeability mainly lower than 0.3 mD. In recent years, there have been few reports on tight oil reservoir with permeability lower than 0.3 mD, though such ultra-low permeability reservoirs have great resource potential. On the basis of high-pressure mercury intrusion experiments, this study uses two models based on water saturation and mercury saturation to calculate the fractal dimension of a tight sandstone reservoir with ultra-low permeability. By analyzing the relationship between the fractal dimension and reservoir physical properties, a calculation method is selected that is suitable for characterizing the pore structures in tight sandstone reservoir with ultra-low permeability. On this basis, the fractal characteristics of different pore structures in tight sandstone reservoirs are also analyzed, and a new method by means of fractal dimensions is proposed to characterize tight sandstone reservoirs with ultra-low permeability. The fractal analysis results can ascertain whether the fractal analysis is suitable for characterizing of tight sandstone reservoirs with ultra-low permeability and are of great importance for quantitatively characterizing the pore structure and heterogeneity of tight sandstone reservoirs. In addition, the results will provide insights into reservoir quality prediction in similar sedimentary backgrounds.

## Geologic settings

The Ordos Basin is a multicyclic superimposed basin in North China and covered an area of  $37 \times 10^4 \text{ km}^2$  (Fig. 1a).

According to its structural characteristic, the Ordos Basin could be subdivided into six structural units, namely, the Yishan Slope, the Yimeng Uplift, the Weibei Uplift, the Jinxi Fault-Fold Belt, the Fault-Fold Belt of West Margin and the Tianhuan Syncline (Fig. 1b). The Upper Triassic Yanchang Formation can be subdivided into nine oil-bearing intervals from bottom to top, called Chang 10 to Chang 1 (Fig. 2a), which records the evolution of lacustrine basin from start to end (Yang et al. 2010; Liu et al. 2013). The studied sandstones are from the Chang 6 member, which can be further divided into 3 sub-members based on the sedimentary cycle, lithological association and marker bed, namely, Chang 6<sub>3</sub>, Chang 6<sub>2</sub>, and Chang 6<sub>1</sub>. This research examines Chang 6<sub>3</sub>, which is mainly composed of dark mudstones, siltstones, and fine sandstones (Fig. 2b).

The study area is located in the Huaqing area in the southwestern of the Yishan Slope in the Ordos Basin, with an area of  $43 \times 10^2 \text{ km}^2$  (Fig. 1b). Anticlines and faults were not developed in most parts of the study area. During Chang 6<sub>3</sub> sub-member deposition, the Huaqing area was located in the mixed district of northeast and southwest provenances. In the southern part of the Huaqing area, there mainly developed sediments corresponding to the semi-deep lake environments and sandy debris flows formed by the collapse of sandbodies in the southwestern braided river delta front, while in the northern part, there dominantly developed gravity flow deposits corresponding to the semi-deep lake environments, which were formed by collapse of sandbodies in the northeastern meandering river delta front. The conditions of steep slope, deep water, and the proximal source supplied by the Qinling Mountains were conducive to the formation of gravity flow deposition (Zheng et al. 2007; Cao et al. 2016). The Chang 6<sub>3</sub> reservoirs are typical ultra-low permeability tight reservoirs with generally poor reservoir properties. The porosity ranges from 1.65 to 18.52% with an average of 9.77%, and the permeability is between 0.001 and 1.89 mD with a mean of 0.21 mD. More than 70% of the core samples show a permeability lower than 0.1 mD.

## Materials and methodology

### Samples and experimental measurements

Nine core plugs were collected in the Chang 6<sub>3</sub> sub-member in the study area. All the samples were carefully packaged and sent to the laboratory immediately for experimental analysis. Before the tests, each core plug sample was washed with a mixture of trichloromethane and alcohol to eliminate residual oil, and then the samples were dried at 110 ° for 24 h under vacuum. To ensure

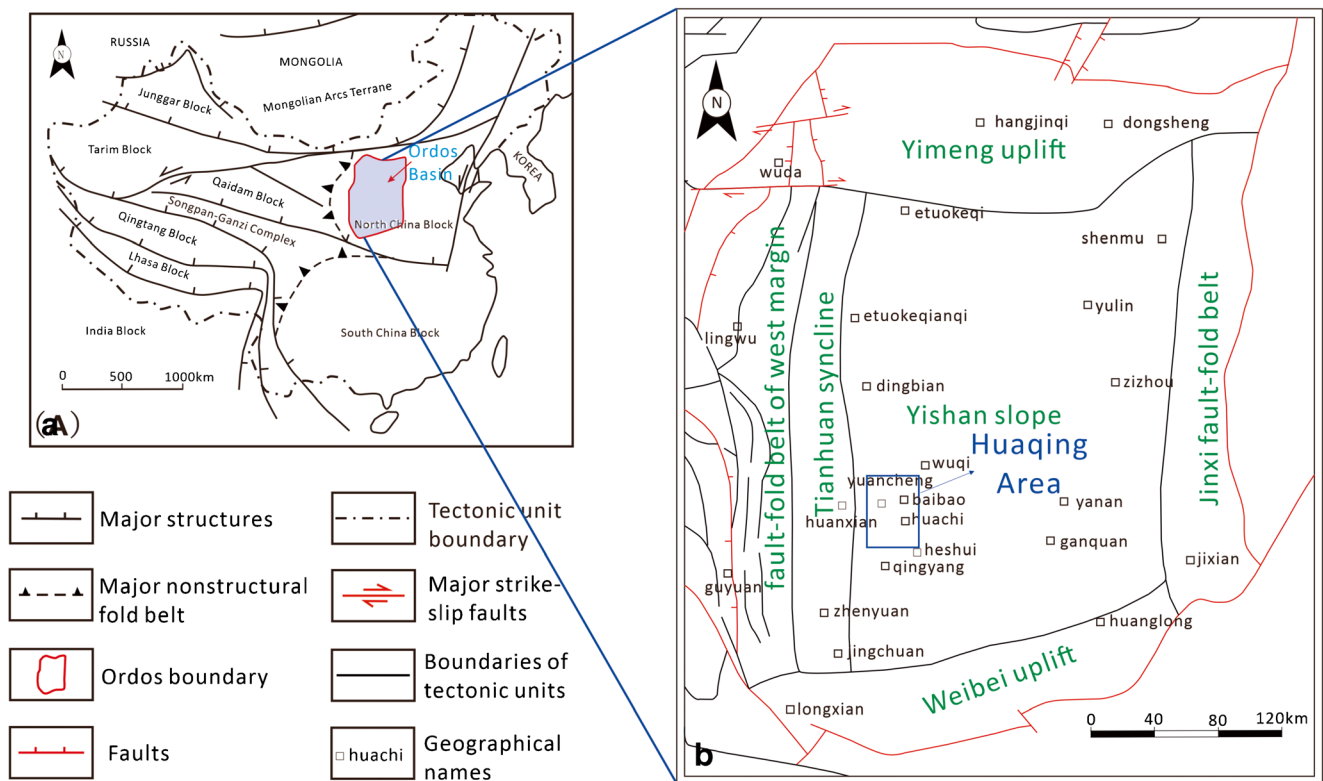


**Fig. 1.** **a** Location map of the Ordos Basin in China (modified from Yang et al. 2005). **b** Simplified structure units and location map of the Huaqing area in the Ordos Basin

the accuracy and comparability of texts, the core plugs were drilled at the same depth of the same well during sampling in sizes of 2.54 cm diameter and 5.00 cm length to obtain uniform samples. These core plugs were used in the manufacture of casting thin section, scanning electron microscopy (SEM) observations, and high-pressure mercury intrusion (HPMI) experiments.

The casting thin section was prepared by vacuum-impregnation with blue-dyed epoxy resin to characterize the pores and throats. Through observations of thin sections, various pore types were determined. All casting thin sections were analyzed by optical polarization microscopy (Olympus BH2). The Merlin scanning electron microscope was used for SEM observation, which was performed by recording the secondary electron image. Prior to analysis, all the samples were coated with carbon to avoid electrostatic charging.

The HPMI experiment was conducted on a Corelab CMS300 mercury porosimeter in accordance with the Chinese SY/T 5346-2005 and SY/T 5336-2006 standards (NDRCC 2005, 2006). HPMI experiment was carried out on the cut core plug (25 × 40 mm cylinder sample), and all core plugs were dried under vacuum at 110 °C for 4 h. The maximum intrusion pressure for HPMI was 200 MPa, and the corresponding pore-throat size was 1.6 nm. Both intrusion and extrusion curves were obtained from the HPMI experiments.

## Methodology

In a certain range, a fractal is a self-similar, virtual geometric object that is completely independent of the magnifications. Previous studies have demonstrated that the pore structures of natural porous sedimentary rocks have fractal features and that the fractal dimension could be determined accordingly (Giri et al. 2012; Kulesza and Bramowicz 2014). It has been considered that a fractal dimension between 2 and 3 corresponds with three-dimensional fractal objects. This physical meaning relates the degree of similarity between the part of the reservoir pore structure and the whole reservoir pore structure, or it is the degree of concentration of the pore size distribution (Katz and Thompson 1985). In a geological sense, the fractal dimension is a comprehensive characterization of the complexity of the reservoir pore structures, and it could be used as an important index to characterize pore structures (Thompson et al. 1987). Generally, the larger the fractal dimension is (closer to 3), the less smooth the pore-throat surface, the worse the sorting, the more complicated the pore size distribution, the poorer the reservoir performance, and the stronger the microscopic heterogeneity; when the fractal dimension is close to 2, the previously mentioned situation was the opposite (Chen and Sun 1996; Gao et al. 2014). Therefore, the fractal dimension was an ideal parameter for describing the pore structure characteristics of reservoirs. Thus, fractal

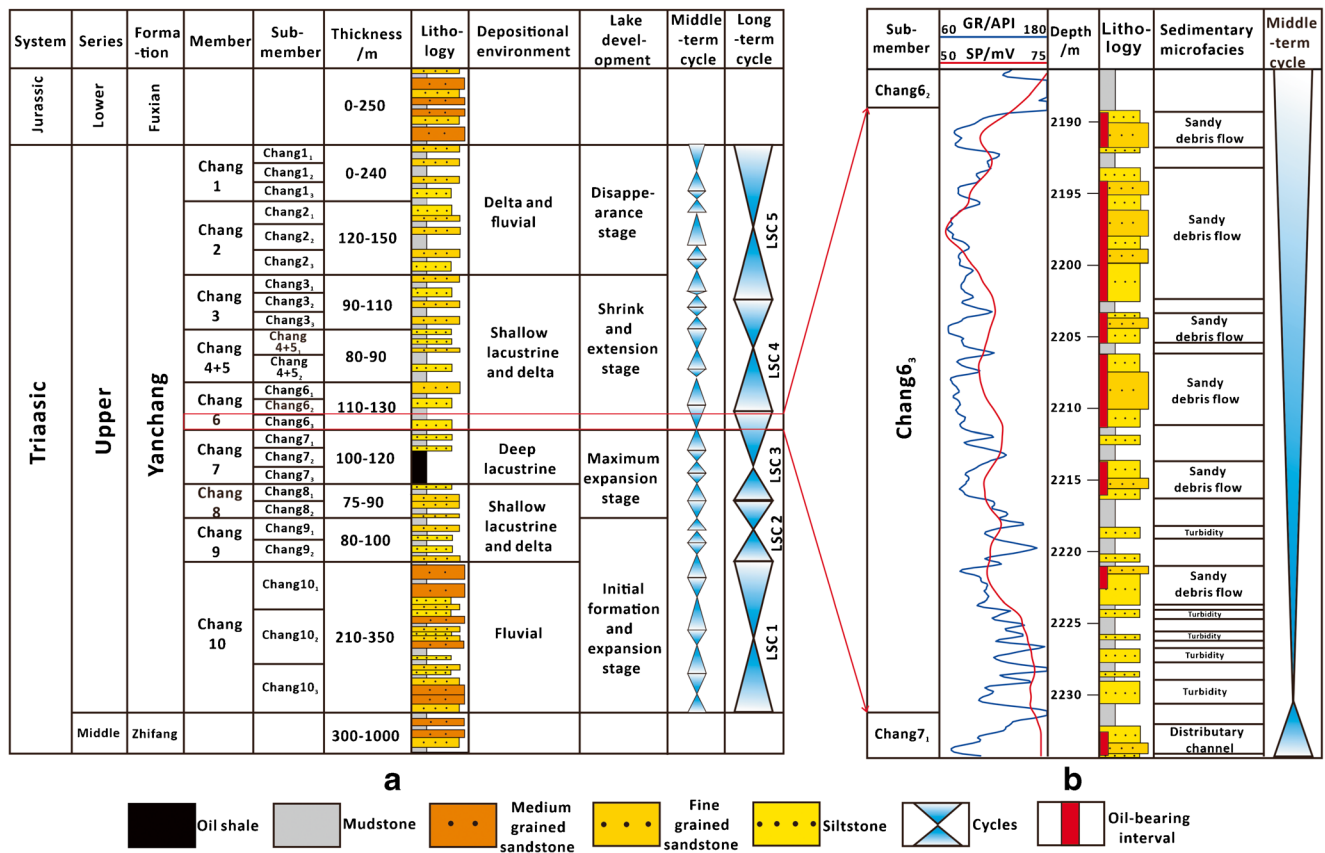


**Fig. 2** The stratigraphic column with focused interval of the Upper Triassic Yanchang Formation in the Ordos basin (modified from Zhou et al. 2016). **a** The whole Yanchang Formation. **b** The Chang 6<sub>3</sub> sub-member of Yanchang Formation

dimensions could reflect the degree of heterogeneity of the pore structure in a reservoir and could provide an effective way to quantitatively characterize the complexity of reservoirs.

Based on fractal geometry theory, a fractal object can be represented by a power-law function (Li 2004):

$$N(r) \propto r^{-D_f} \tag{1}$$

where  $N(r)$  is the number of a fractal object whose characteristic linear dimensions are larger than  $r$ ,  $\alpha$  represents “proportional to,”  $r$  is the radius of a fractal object, and  $D_f$  is the fractal dimension.

At present, there are two main methods for calculating the fractal dimension based on mercury injection capillary pressure curves: the water saturation (wetting phase) method and the mercury saturation (nonwetting phase) method (Friesen and Mikula 1987; Li 2010; Gao et al. 2014).

The mercury saturation method is as follows (Li 2010; Lai and Wang 2015):

Based on the capillary model,  $N(r)$  can be expressed as follows:

$$N(r) = \frac{V_{Hg}}{\pi r^2 l} \tag{2}$$

where  $l$  is the length of the capillary and  $V_{Hg}$  is the cumulative volume of mercury flowing through the capillary with radius  $r$ .

According to the Laplace law, the pore radius  $r$  is related to capillary pressure:

$$P_c = \frac{2\sigma \cos\theta}{r} \tag{3}$$

where  $P_c$  is the capillary pressure,  $\theta$  is the contact angle, and  $\sigma$  is the surface tension.

From Eq. (1)-(3), Eq. (4) can be obtained:

$$V_{Hg} \propto P_c^{-(2-D_f)} \tag{4}$$

According to the definition of mercury saturation in rock samples:

$$S_{Hg} = \frac{V_{Hg}}{V_p} \tag{5}$$

where  $S_{Hg}$  is mercury saturation, and  $V_p$  is the total pore volume of the sample.

Combining Eq. (4) and Eq. (5):

$$S_{Hg} = \alpha P_c^{-(2-D_f)} \tag{6}$$

where  $\alpha$  is a constant.

Taking logarithms on both sides of Eq. (6) and making simple transformations:

$$\log S_{Hg} = (D_f - 2) \log P_c + \log \alpha \tag{7}$$

The water saturation method is as follows (He and Hua 1998):

Based on fractal geometry,  $N(r)$  can be expressed as follows:

$$N(> r) = \int_r^{r_{max}} f(r) dr = m r^{-D_f} \tag{8}$$

where  $f(r)$  is the density function of the pore size distributions,  $r_{max}$  is the maximum pore radius,  $m$  is a constant.

Differentiating Eq. (8):

$$f(r) = \frac{dN(r)}{dr} = -D_f m r^{-D_f - 1} \tag{9}$$

After substituting and then integrating Eq. (9) into Eq. (10), Eq. (11) can be obtained:

$$V(< r) = \int_{r_{min}}^r f(r) n r^3 dr \tag{10}$$

$$V(< r) = \frac{mn D_f}{3 - D_f} (r^{3 - D_f} - r_{min}^{3 - D_f}) \tag{11}$$

where  $V(< r)$  is the accumulated pore volume,  $r_{min}$  is the minimum pore radius, and  $n$  is a constant that links to the pore structures ( $n=1$  when the pore shape is a cube,  $n=4\pi/3$  when the pore shape is a sphere).

Therefore, we can obtain the total pore volumes in the same method, which can be expressed as follows:

$$V = -\frac{mn D_f}{3 - D_f} (r_{max}^{3 - D_f} - r_{min}^{3 - D_f}) \tag{12}$$

Substituting Eq. (11) and Eq. (12):

$$S = \frac{V(< r)}{V} = \frac{r^{3 - D_f} - r_{min}^{3 - D_f}}{r_{max}^{3 - D_f} - r_{min}^{3 - D_f}} \tag{13}$$

where  $S$  is the accumulated pore volume fraction.

When  $r_{min} \ll r_{max}$ , Eq. (13) can be rearranged as follows:

$$S = \left( \frac{r}{r_{max}} \right)^{3 - D_f} \tag{14}$$

Substituting Eq. (3) into Eq. (14):

$$S_w = \left( \frac{P_c}{P_{min}} \right)^{D_f - 3} \tag{15}$$

where  $S_w$  is the wetting phase saturation (the wetting phase is water in this study) in the reservoirs when the capillary pressure is  $P_c$ ,  $P_{min}$  is the pressure corresponding to the pore radius  $r$ ,

and  $P_{min}$  is the capillary pressure corresponding to the maximum pore radius  $r_{max}$  in reservoirs, i.e., the threshold capillary pressure.

Taking logarithms on both sides of Eq. (15) and making simple transformations:

$$\log S_w = (3 - D_f) \log P_{min} + (D_f - 3) \log P_c \tag{16}$$

Equations (7) and (16) indicate that if the reservoir pore structure has fractal properties, there is a linear relationship between  $\log S_{Hg} - \log P_c$  and  $\log S_w - \log P_c$ , and the fractal dimension can be calculated according to its slope:

$$D_{f1} = S_1 + 2 \tag{17}$$

$$D_{f2} = S_2 + 3 \tag{18}$$

where  $D_{f1}$  is the fractal dimension based on the calculation of mercury saturation,  $S_1$  is the slope of  $\log S_{Hg} - \log P_c$  plot,  $D_{f2}$  is the fractal dimension based on the calculation of water saturation, and  $S_2$  is the slope of  $\log S_w - \log P_c$  plot.

## Results

### Petrography characteristics

According to the observations and statistical results of casting thin sections under the microscope (Table 1), these samples are characterized by silt to fine size, poorly sorted, and subrounded to subangular grains. The tight sandstones are rich in feldspars (av. 29.80%) and are less rich in quartz (av. 28.91%) and rock fragments (av. 17.40%). Lithic arkose and feldspathic are the dominant types of these tight sandstones.

### High-pressure mercury intrusion

In the HPMI test, the mercury injection saturation is obtained by the conversion of the mercury injection volume, and the distribution curves of the pore-throat size are calculated according to the mercury injection curves. The HPMI curves of 9 samples are shown in Fig. 3. From the HPMI test, parameters that reflect the pore-throat size (such as maximum pore-throat radius, average pore-throat radius, and medium pore-throat radius), pore-throat distribution (such as sorting coefficient) and pore-throat connectivity (such as threshold pressure, medium saturation pressure, maximum mercury injection saturation and mercury extrusion efficiency) can be obtained (Table 2). The maximum pore-throat radius ( $R_d$ ) is between 0.053 and 2.785  $\mu$  with a mean of 0.687  $\mu$ ; the medium pore-throat radius ( $R_{50}$ ) is in the range of 0.006 to 1.479  $\mu$  with a mean of 0.224  $\mu$ ; the average pore-throat radius ( $R_a$ ) ranges from 0.012 to 1.147  $\mu$  with a mean of 0.215  $\mu$ . This indicates that most of the pore-throat sizes are small (less than 1  $\mu$ p) in these tight sandstone samples. The sorting

**Table 1** Mineralogical composition contents of the Chang 6<sub>3</sub> tight sandstones

Well name	Depth/ m	Lithology	Detrital component content/%			Carbonate cement/%	Clay minerals/%
			Quartz	Feldspar	Rock fragments		
B40	2260.2	Fine sandstone	20	33.4	20.1	6.3	20.2
L320	2163.5	Siltstone	34.4	18.2	17.2	6.4	23.8
L330	2199.9	Siltstone	37.9	16.7	22.2	5.3	17.9
Y293	2179.2	Siltstone	28.6	32.4	14.9	6.2	17.9
Y299	1958.6	Siltstone	27.6	36.1	15.6	8.2	12.5
Y414	2009.9	Fine sandstone	31.4	29.6	14.4	5.2	19.4
Y416	2164.5	Siltstone	29	34.7	13	1.8	21.5
Y432	2042.2	Fine sandstone	30.2	38.9	17.4	6.7	6.8
Y438	2230.4	Siltstone	21.1	28.2	21.8	6.7	22.2

coefficient (SC) is in the range of 1.137 to 2.698 with a mean of 1.839, which implies that the pore-throat size is quite different and that the pore distributions are highly heterogeneous. The threshold pressure ( $P_d$ ) varies from 0.264 to 13.788 MPa with a mean of 4.770 MPa, and more than half of the samples are greater than 2 MPa; meanwhile, the medium saturation pressure ( $P_{50}$ ) varies from 0.503 to 123.291 MPa with a mean of 32.278 MPa; the mercury extrusion efficiency (ME) is between 23.94 and 66.44%, with a mean of 37.16%. This shows that the pore-throat connectivity in the study area is poor. In summary, the pore structures of tight sandstone reservoirs in the study area are complex and heterogeneous.

Based on the shape of the mercury injection curves, referring to reservoir physical property data and mercury injection parameters (Table 2), the pore structures of 9 tight sandstones samples are divided into 4 types, namely, type 1, type 2, type 3, and type 4 (Fig. 4). There are several differences between these 4 types of pore structures. As the type of pore structure changes from type 1 to type 4, several differences are observed. The distribution of the mercury injection curve moves gradually to the northeast (Fig. 4).

The threshold pressure ( $P_d$ ) and medium saturation pressure ( $P_{50}$ ) gradually increase, while the maximum pore-throat radius ( $R_d$ ) and medium pore-throat radius ( $R_{50}$ ) gradually decrease (Table 2). The permeability decreases as the pore-throat radius decreases (Table 2). The different types of samples have different pore-throat size distributions (Fig. 5). From type 1 to type 4, the peak values of pore-throat size distributions are moving from right to left in the graph, and the peak values of 8 samples are less than  $1.0 \mu\text{m}$ . Thus, the pore-throat systems in the study area are dominated by small pore-throat sizes.

## Fractal dimensions

The  $\log S_{Hg} - \log P_c$  and  $\log S_w - \log P_c$  intersection curves of the 9 tight sandstone samples, which are plotted by the methods mentioned in “Methodology,” are shown in Figs. 6

and 7, and the results show that all curves fit well (the correlation coefficient  $R^2$  is greater than 0.90). This indicates that these samples are fractal as a whole and can be characterized by fractal geometry theory. However, the fractal characteristic curves based on the mercury saturation method and water saturation method are quite different, and the characteristics of these two methods are analyzed separately below.

## Mercury saturation method

As we can see in Fig. 6, with the exception of two type 4 samples (Y299 and L320) that can be fitted by one straight line, most samples need to be fitted by two straight lines with different slopes (there is a clear turning point that breaks the curve into two segments, corresponding to the larger pore-throat sizes and the smaller pore-throat sizes). Samples with larger pore-throat sizes (corresponding to low capillary pressures) tend to have higher slopes, while samples with smaller pore-throat sizes (corresponding to high capillary pressures) are likely to have lower slopes, which indicates that the different ranges of pore-throat size distributions have different fractal dimensions, i.e., the fractal dimensions of larger and smaller pore-throat sizes are different. The fractal dimension of each segment can be calculated by the slope of each fitted straight line, and then the total fractal dimension of each sample is obtained with the weighted average of mercury saturation in the larger pore-throat and smaller pore-throat sizes, which ranges from 2.122 to 2.947 with a mean of 2.622 (Table 3). The dispersed distributions indicate that the pore-throat systems in tight sandstone reservoirs are heterogeneous and complex.

Figure 7 shows that the fractal dimension calculated by the mercury saturation method has a good correlation with the reservoir porosity, permeability and pore structure parameters (i.e., threshold pressure and pore-throat radius), with the correlation coefficient reaching 0.688, 0.839, 0.817, and 0.855, respectively. With increasing fractal dimensions, porosity and permeability gradually decrease and pore structure parameters

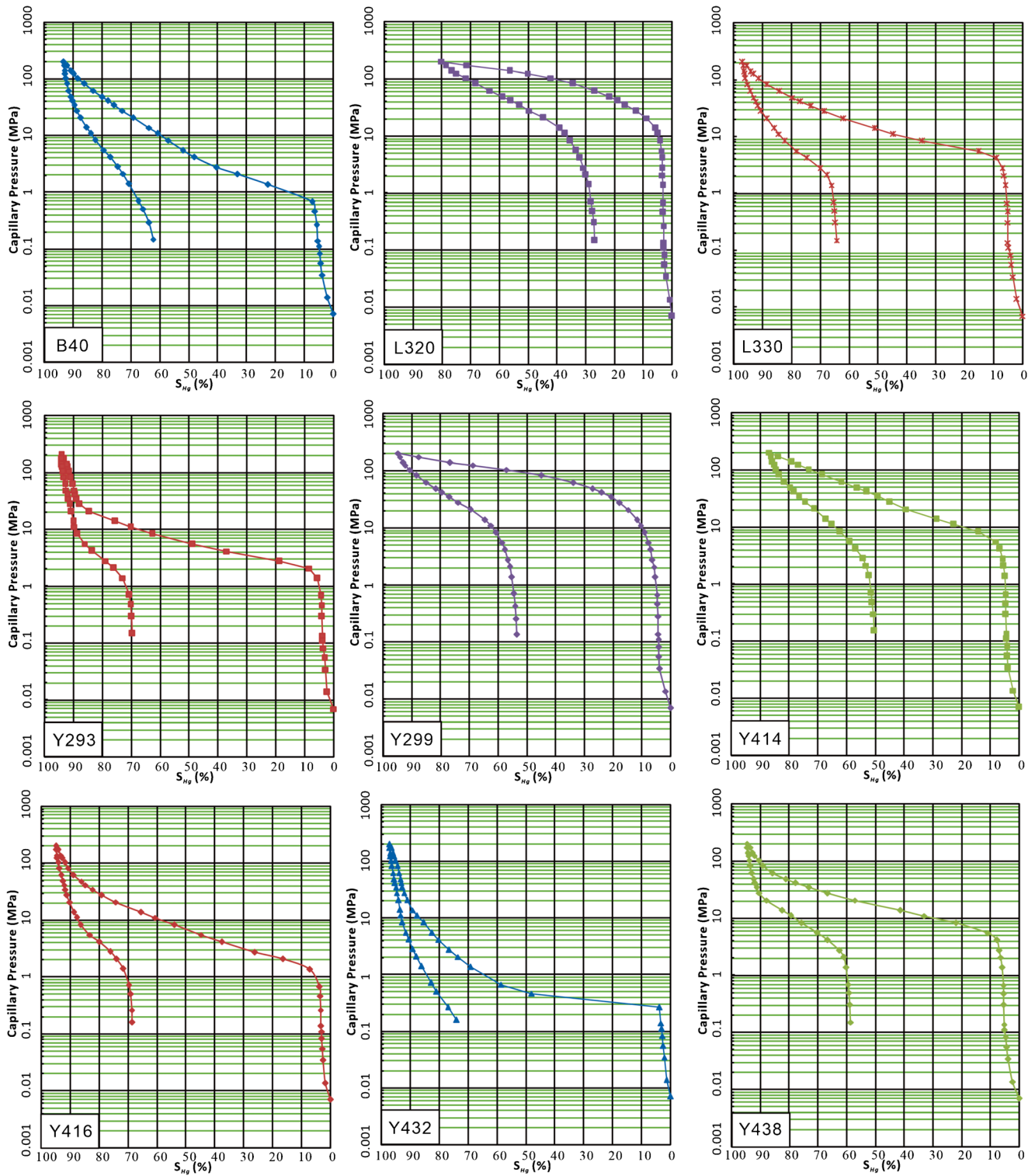


Fig. 3 HPMI-derived mercury injection and extrusion curves for nine tight sandstone samples

become worse. Therefore, the fractal dimension calculated by this method can quantitatively describe the complexity of pore structure to a certain extent and can better realize the classification and evaluation of pore structure in tight sandstone reservoirs.

**Water saturation method**

Figure 8 shows that the fractal characteristic curves based on the water saturation method are quite different from those based on the mercury saturation method. Only two samples

**Table 2** HPMI parameters of the Chang 6<sub>3</sub> tight sandstones

Type	Samples	Depth/ m	$\varphi$ /%	K/ mD	$P_{50}$ / Mpa	$P_d$ / Mpa	$R_{50}$ / $\mu\text{m}$	$R_a$ / $\mu\text{m}$	$R_d$ / $\mu\text{m}$	SC	$S_m$ /%	$S_r$ /%	ME/%
1	Y432	2042.2	11.33	1.817	0.503	0.264	1.479	1.147	2.785	2.384	97.200	73.930	23.941
2	B40	2260.2	9.01	0.197	4.817	0.677	0.156	0.269	1.085	2.698	93.263	62.281	33.221
	Y416	2164.5	9.95	0.081	7.055	0.675	0.109	0.192	1.089	2.217	94.924	68.473	27.865
	Y293	2179.2	8.51	0.041	5.730	1.361	0.132	0.148	0.540	1.806	94.264	69.735	26.022
3	L330	2199.9	6.87	0.026	13.198	2.739	0.057	0.065	0.268	1.724	96.931	64.457	33.502
	Y438	2230.4	5.74	0.012	17.540	4.129	0.044	0.051	0.178	1.585	94.684	58.647	38.060
4	Y414	2009.9	3.01	0.006	35.980	5.516	0.021	0.038	0.133	1.798	86.692	50.385	41.881
	Y299	1958.6	2.54	0.003	91.392	13.779	0.009	0.011	0.053	1.205	94.804	53.546	43.519
	L320	2163.5	1.38	0.006	123.291	13.788	0.006	0.012	0.053	1.137	80.067	26.875	66.435

$\varphi$ : gas measurement porosity;  $K$ : gas measurement permeability;  $P_d$ : threshold pressure;  $P_{50}$ : medium saturation pressure;  $R_d$ : maximum pore-throat radius;  $R_a$ : average pore-throat radius;  $R_{50}$ : medium pore-throat radius;  $SC$ : sorting coefficient;  $S_r$ : residual mercury saturation;  $S_m$ : maximum mercury injection saturation;  $ME$ : mercury extrusion efficiency

of type 4 (Y299 and L320) are fitted by two straight lines with different slopes, while other samples can be fitted by one straight line, which is in contrast to the results based on the mercury saturation method. The fractal dimension calculated by the water saturation method ranges from 2.197 to 2.560, with a mean of 2.401, and is smaller than the results from the mercury saturation method.

Figure 9 shows that the fractal dimensions calculated by the water saturation method have poor correlations with reservoir porosity, permeability and pore structure parameters (i.e.,

threshold pressure and pore-throat radius), with correlation coefficients of 0.010, 0.162, 0.087, and 0.106, respectively. With increasing fractal dimensions, porosity and permeability tend to increase, which is in contrast to the fractal principle: the larger the fractal dimension is, the poorer the reservoir performance. Therefore, the fractal dimension calculated by the water saturation method cannot reflect reservoir physical properties, and it cannot reflect the heterogeneity of pore-throat systems. In other words, compared with the mercury saturation method, the water saturation method is not suitable for characterizing the pore structures of tight sandstone reservoirs with ultra-low permeability.

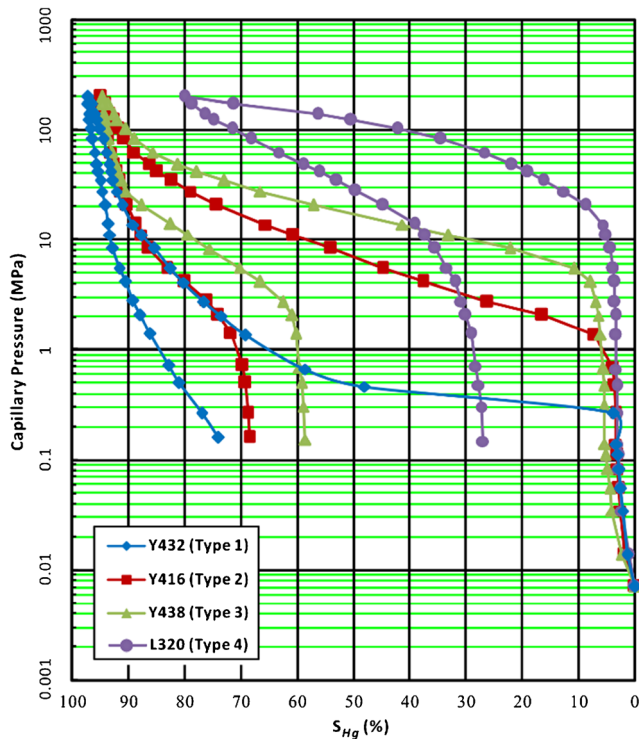


**Fig. 4** Four types of mercury injection and extrusion curves derived from HPMI. Y432 (type 1),  $\varphi = 11.33\%$ ,  $K = 1.817$  mD. Y416 (type 2),  $\varphi = 9.95\%$ ,  $K = 0.081$  mD. Y438 (type 3),  $\varphi = 5.74\%$ ,  $K = 0.012$  mD. Y320 (type 4),  $\varphi = 1.38\%$ ,  $K = 0.006$  mD

## Discussion

### Comparison between the mercury saturation method and the water saturation method

Previous studies have pointed out that pore structures of reservoirs had good fractal characteristics in the range of 0.2–50.0  $\mu\text{r}$  (Katz and Thompson 1985; Krohn 1988), and He and Hua (1998) deduced the formula for calculating the fractal dimension of rock samples by using the relationship between fluid saturation of the wetting phase and capillary pressure. However, the fractal dimension calculated by the wetting phase (water) cannot quantitatively characterize the pore structures of tight sandstone reservoirs with ultra-low permeability in this work. The possible reasons are as follows:

- 1 Strong diagenesis leads to generally smaller pore-throat systems in tight sandstone reservoirs. Reservoirs in the study area of the Triassic Yanchang Formation are characterized by poorly sorted, subangular grains in silt to fine sizes, resulting in a reservoir with poor original porosity and permeability, and this reservoir has undergone strong



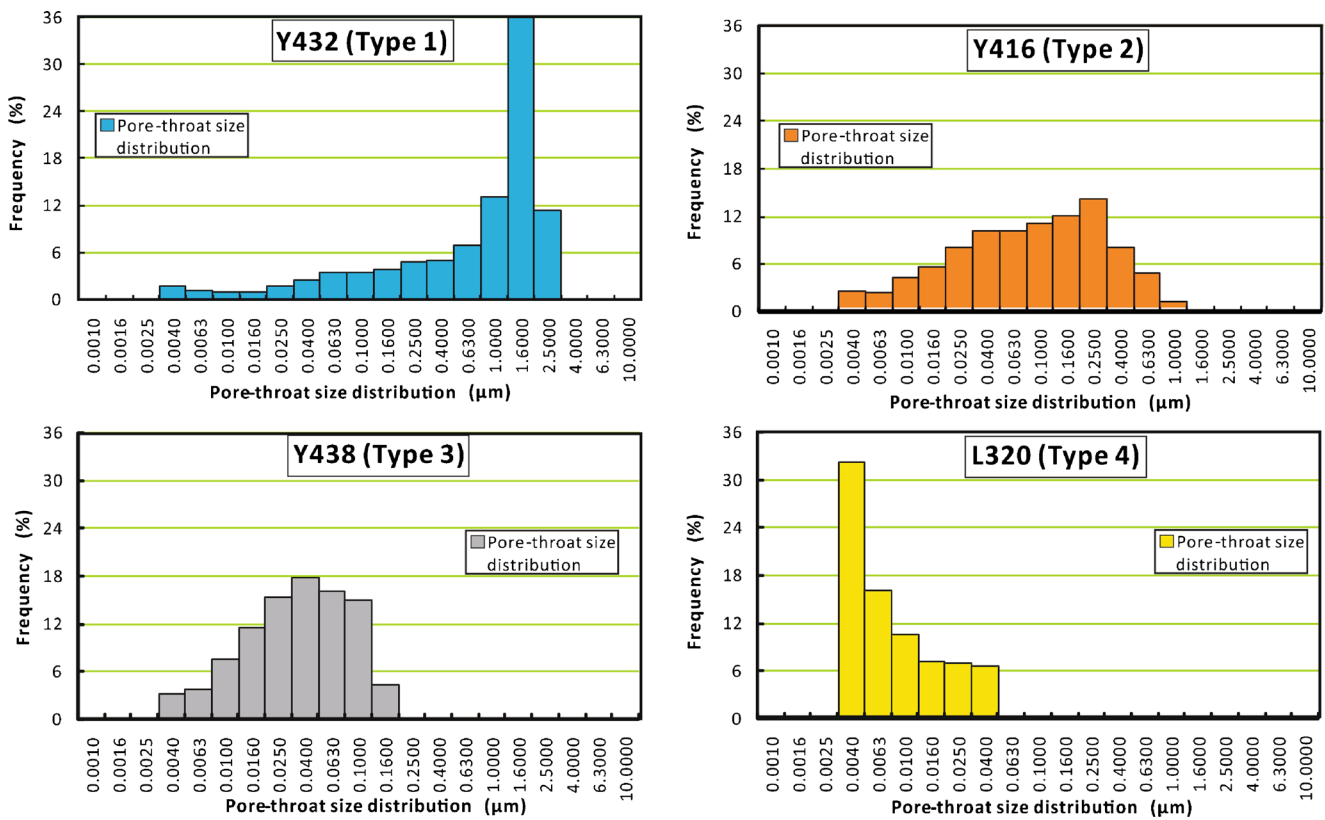


**Fig. 5** Four types of pore-throat size distributions derived from HPMI. Y432 (type 1),  $\phi = 11.33\%$ ,  $K = 1.817$  mD. Y416 (type 2),  $\phi = 9.95\%$ ,  $K = 0.081$  mD. Y438 (type 3),  $\phi = 5.74\%$ ,  $K = 0.012$  mD. Y320 (type 4),  $\phi = 1.38\%$ ,  $K = 0.006$  mD

and complex diagenesis during a long geological history. In the process of its evolution, typical tight sandstone reservoirs with ultra-low permeability are ultimately formed. Strong compaction results in a smaller pore-throat radius of the reservoirs, and the maximum pore-throat radius only ranges from 0.053 to 2.785 μm with a mean of 0.687 μm. This leads to the fact that  $r_{min} < r_{max}$  in the derivation of Eq. (14) is not fully valid. Therefore, the fractal dimension calculated by the water saturation method has a large deviation, while the fractal dimension calculated by the mercury saturation method is not restricted by this condition.

- The bound water saturation is high in tight sandstone reservoirs. The water saturation  $S_w$  and mercury injection saturation  $S_{Hg}$  in the calculation of fractal dimension represent the proportion of pores with radius sizes less than  $r$  and radius sizes greater than  $r$  with respect to total pore space, respectively. Because the pore-throat sizes of the tight sandstone reservoirs with ultra-low permeability are mostly tiny, water does not easily flow into it (i.e., bound water). Therefore, a larger mercury intrusion pressure is required for mercury to displace the bound water in such pore-throat systems. The fractal dimension, which is calculated by the water saturation method, includes this part of the pore throats for each data point, resulting in deviations in the calculated results; in addition, there are no such

problems in large pores (most of the data points calculated based on the mercury saturation method do not include this part of the pore throats). Li et al. (2018a, b) used NMR experiments to study the movable fluids in this study area, and the results showed that the bound water saturation was in the range of 44.06–97.84%, with a mean of 72.52%. Table 2 shows that the maximum mercury injection saturation ranges from 80.07 to 97.20%, with a mean of 92.54%. The higher the mercury injection saturation of the samples is, the more bound water that needs to be discharged, and the greater the calculation error. Therefore, the high bound water saturation of reservoirs is also one of the reasons for the inaccurate fractal dimension calculated by the water saturation method.

In summary, for ultra-low permeability tight sandstone reservoirs with strong heterogeneity and complicated diagenesis, the mercury saturation method rather than the water saturation method should be chosen to calculate the fractal dimension.

### Fractal characteristics of tight sandstone reservoirs

As previously described, compared with the mercury saturation method, the water saturation method is not suitable for tight sandstone reservoirs with ultra-low permeability.

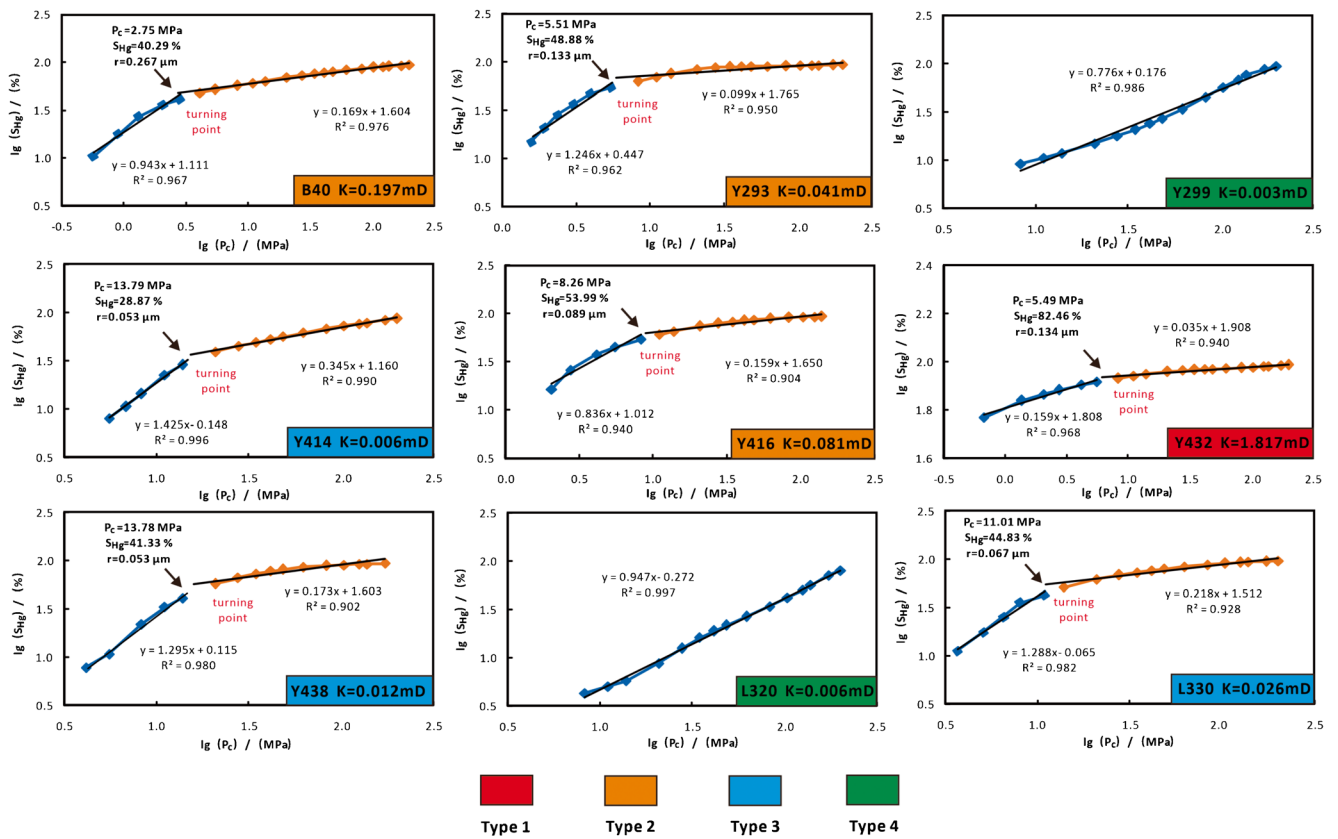


**Fig. 6** Fractal characteristic curves of 9 tight sandstone samples based on the mercury saturation method. A double-logarithm coordination showing the relationship between the capillary pressure ( $P_c$ , MPa) and the mercury saturation ( $S_{Hg}$ , %)

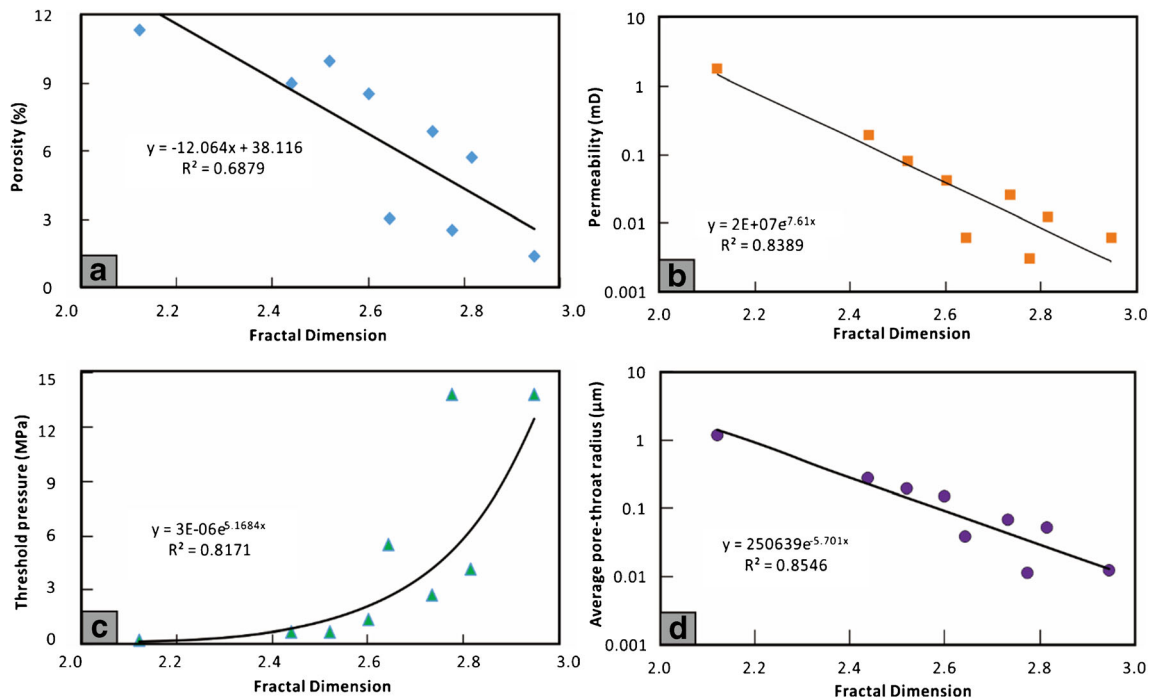


**Fig. 7** The plots show the relationships between the fractal dimension based on the mercury saturation method and **a** porosity, **b** permeability, **c** threshold pressure, **d** average pore-throat radius

**Table 3** Fractal dimensions of 9 tight sandstone samples based on the mercury saturation method ( $D_{f1}$ ) and the water saturation method ( $D_{f2}$ )

Type	Samples	Depth/m	$\phi$ /%	K/mD	Range of pore-throat size distribution/ $\mu\text{m}$	$D_{f1}$	$D_{f1}$ final	$D_{f2}$	$D_{f2}$ final
1	Y432	2042.2	11.33	1.817	0.134-1.100 0.004-0.134	2.159	2.122	2.56	2.56
	B40	2260.2	9.01	0.197	0.178-1.085 0.004-0.178	2.943	2.439	2.548	2.548
2	Y416	2164.5	9.95	0.081	0.089-0.357 0.004-0.089	2.836	2.52	2.368	2.368
	Y293	2179.2	8.51	0.041	0.133-0.357 0.004-0.133	3.246	2.601	2.389	2.389
	L330	2199.9	6.87	0.026	0.067-0.268 0.004-0.067	3.288	2.735	2.197	2.197
3	Y438	2230.4	5.74	0.012	0.053-0.268 0.004-0.053	3.295	2.815	2.203	2.203
	Y414	2009.9	3.01	0.006	0.053-0.179 0.004-0.053	3.425	2.644	2.515	2.515
	Y299	1958.6	2.54	0.003	0.004-0.012 0.012-0.133	2.776	2.776	2.839	2.305
4	L320	2163.5	1.38	0.006	0.004-0.012 0.012-0.134	2.947	2.947	2.87	2.526
								2.361	

Therefore, fractal curves and fractal dimensions obtained by the mercury saturation method are used to analyze the fractal

characteristics of tight sandstone reservoirs with ultra-low permeability.

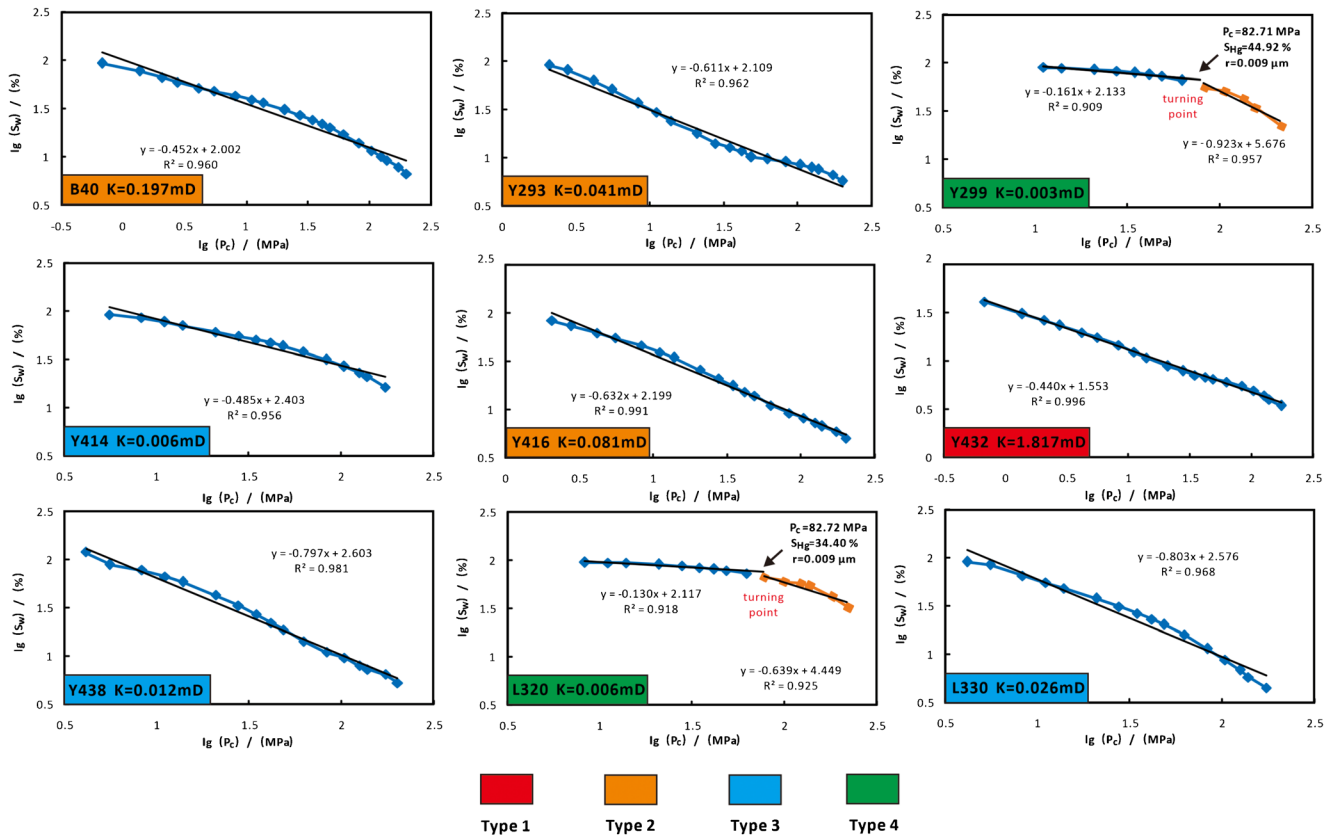


**Fig. 8** Fractal characteristic curves of 9 tight sandstone samples based on the water saturation method. A double-logarithm coordination showing the relationship between the capillary pressure ( $P_C$ , MPa) and the water saturation ( $S_W$ , %),  $S_W = 1 - S_{Hg}$

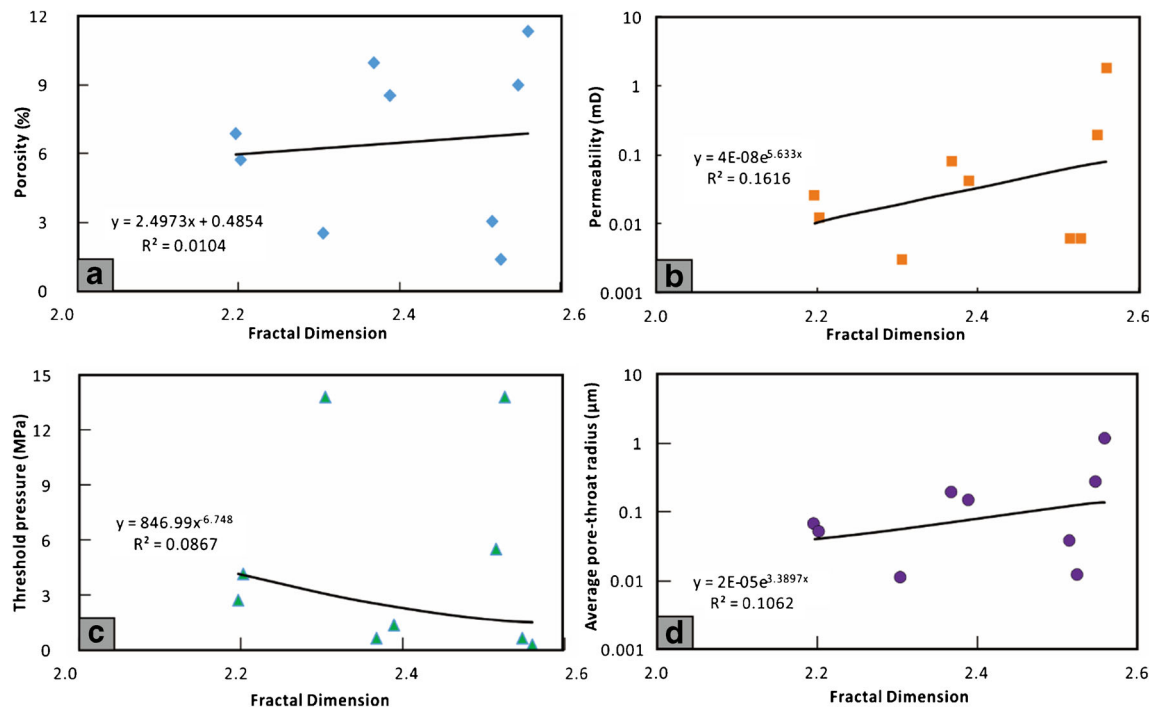


**Fig. 9** The plots show the relationships between the fractal dimension based on the water saturation method and **a** porosity, **b** permeability, **c** threshold pressure, **d** average pore-throat radius

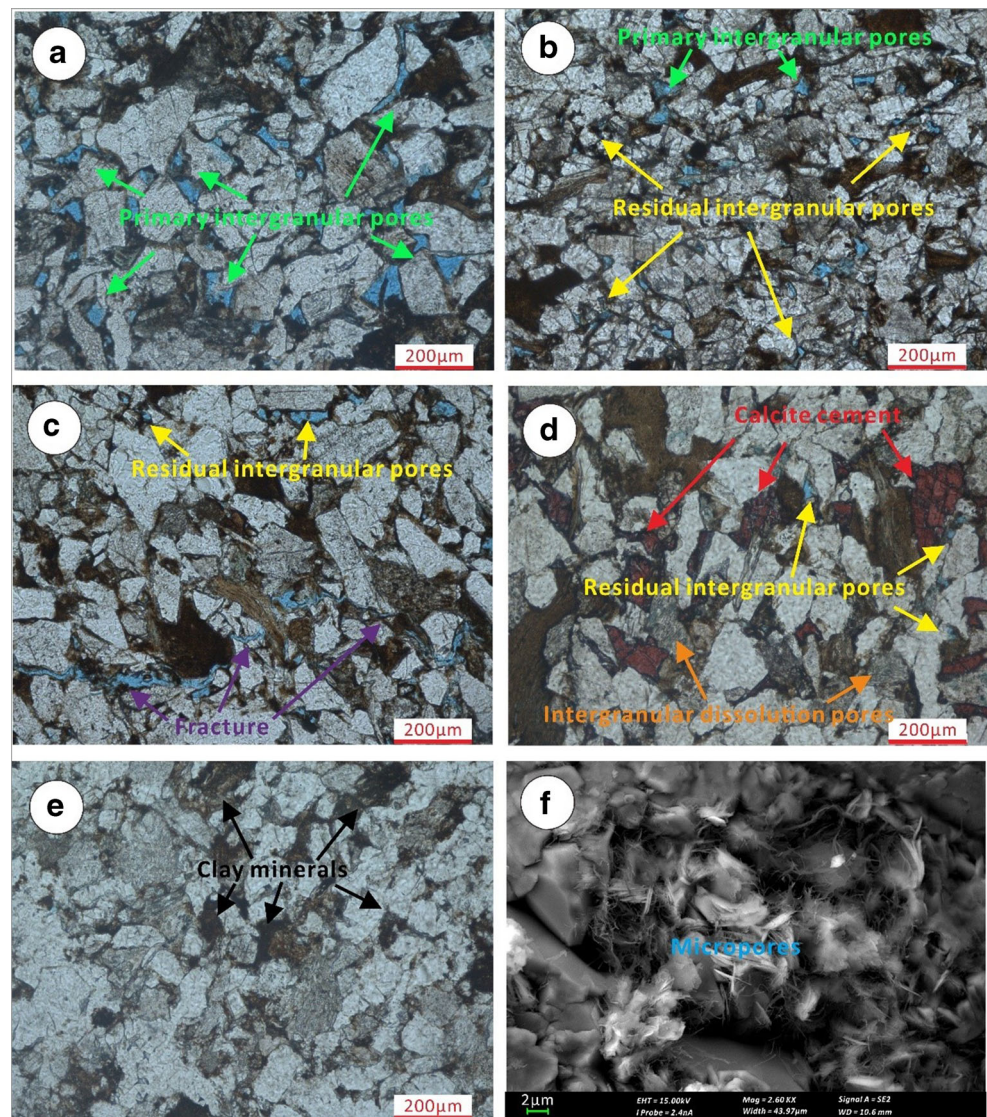
Figure 6 and Table 3 show that different reservoir types have different fractal characteristics. For type 4, the data could be fitted by one straight line; in addition, for type 1 to type 3, there is a clear turning point that breaks the curve into two segments, so the data need to be fitted by two straight lines with different slopes (Fig. 6). The pore-throat radius corresponding to the turning point ( $r_{tr}$ ) varies from 0.053 to 0.267  $\mu$  with a mean of 0.114  $\mu$ , which indicates that the turning point divides the pore-throat sizes in tight sandstone reservoirs into two parts: one is the relatively large pore-throat with a radius greater than  $r_{tr}$ , and the other is the relatively small pore-throat with a radius less than  $r_{tr}$ .

Sample Y432 of type 1 has the highest reservoir physical properties among the four types, with a porosity of 11.33% and permeability of 1.817 mD, and the fractal dimensions of large pore-throat and small pore-throat sizes are both close to 2.0, with values of 2.159 and 2.035, respectively (Table 3). These results indicate that both of these types of pore-throat sizes are more uniform and that the reservoirs have better pore structures. The casting thin sections show that the main pore types in type 1 are primary intergranular pores and residual intergranular pores with regular shapes (Fig. 10a); compaction is weak, and cementation is not developed, resulting in no cements occupying the intergranular pores. Therefore, the sample with two low fractal dimensions represents that both large and small pore-throat sizes have weak pore-throat heterogeneity, which reflects that the tight sandstone reservoirs have better pore structures, higher reservoir permeability,

weak compaction and cementation, and more pores with regular shapes (Fig. 11).

Samples B40, Y416, and Y293 of type 2 have medium reservoir physical properties among the four types. The porosity varies from 8.51 to 9.95% with a mean of 9.16%, and the permeability varies from 0.041 to 0.197 mD with a mean of 0.106 mD. In contrast to those of type 1, the fractal dimensions of the large pore-throat and small pore-throat sizes vary greatly, with mean values of 3.008 and 2.142, respectively (Table 3). These two types of pore-throat sizes differ greatly, and larger pore-throat sizes have more complex pore structures than smaller pore-throat sizes. The casting thin sections show that the pore types are dominated by residual intergranular pores, while primary intergranular pores are less dominant. The compaction is obviously stronger than type 1, resulting in the decrease in volume and irregular shape of many intergranular pores (Fig. 10b), which is the main reason for the larger fractal dimension of the large pore-throat sizes. In addition, the existence of fractures (Fig. 10c) might significantly affect the fractal characteristics of pore structures in tight sandstone reservoirs (Lai and Wang 2015), which is also one of the important reasons for the larger fractal dimension of large pore-throat sizes. Although small pore-throat sizes with a radius less than 0.1  $\mu$  have low fractal dimensions, weak heterogeneity, and better pore structures, their pore spaces are so small that the contribution to the storage and seepage of oil and gas resources could be negligible.

**Fig. 10** Casting thin section photomicrographs and scanning electron microscope (SEM) photographs of pore types in the tight sandstone reservoirs. **a** Casting thin section (plane-polarized light, and the same below) image showed the primary intergranular pores between clastic grains (Y432, 2042.2 m). **b** Casting thin section image showed the primary intergranular pores and residual intergranular pores (Y293, 2179.2 m). **c** Casting thin section image showed the residual intergranular pores and fracture (Y416, 2164.5.4 m). **d** Casting thin section image showed almost all intergranular pores were filled with calcite cements; in addition, a few intragranular dissolution pores could be observed (Y414, 2009.9 m). **e** Casting thin section image showed lots of clay minerals matrix and strong compaction made intergranular pores disappeared (L320, 2163.5 m). **f** SEM image showed micropores occurred as a group filling in the clay minerals (Y299, 1958.6 m)



Samples L330, Y438, and Y414 of type 3 have poor physical properties among the four types. The porosity ranges from 3.01 to 6.87% with a mean of 5.21%, and the permeability ranges from 0.006 to 0.026 mD with a mean of 0.015 mD. Similar to type 2, the fractal dimensions of the large pore-throat and small pore-throat sizes vary greatly, with mean values of 3.336 and 2.245, respectively (Table 3). The results show that there is a great difference between the two types of pore-throat sizes as well as the type 2 samples, and the large pore-throat sizes have more complex pore structures than the small pore-throat sizes. The casting thin sections show that the pore types are dominated by residual intergranular pores, while intragranular dissolution pores are less dominant (Fig. 10d). In contrast with the type 2 samples, cementation and dissolution are well developed in the type 3 samples, and from the casting thin section images, it can be found that many intergranular pores are filled with calcite cements (Fig. 10d). Due to the large amount of pore space occupied by calcite

cements, the volume of residual intergranular pores decreases, and the shape becomes irregular. In addition, most of the intragranular dissolution pores are irregular pores generated by selective dissolution of clastic particles, which ultimately results in complex pore structures in tight sandstone reservoirs and large fractal dimensions of large pore-throat sizes. However, similar to the type 2 samples, the fractal dimensions of the small pore-throat sizes with radii less than 0.1  $\mu\text{e}$  are close to 2.0, which indicates better pore structures.

Although the large pore-throat sizes of the reservoirs with type 2 and type 3 samples both have larger fractal dimensions, their diagenesis is different. Type 2 is caused by strong compaction, resulting in irregular pore-throat shapes, complex pore structures, and strong reservoir heterogeneity; type 3 is caused by strong cementation and selective dissolution of particles. Therefore, samples with the high fractal dimensions of large pore-throat sizes but low fractal dimensions of small pore-throat sizes reflect that the reservoirs had complex pore

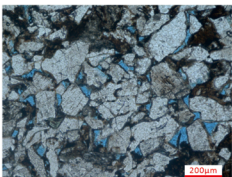
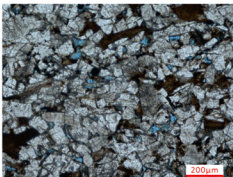
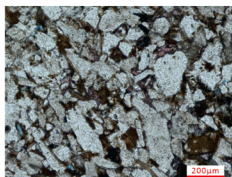
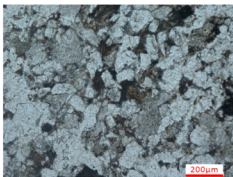
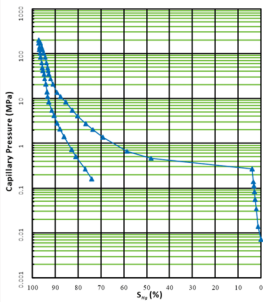
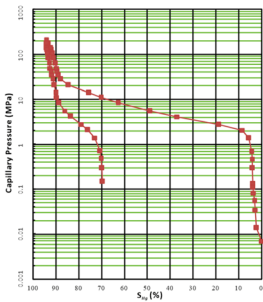
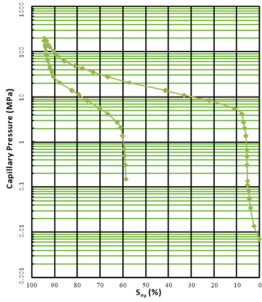
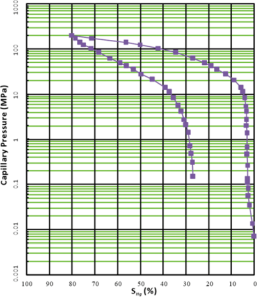
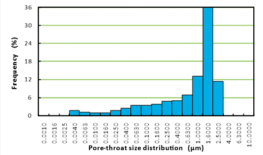
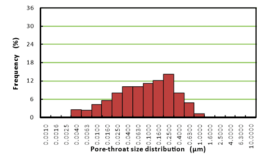
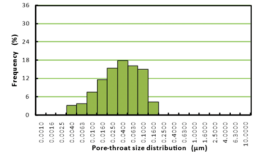
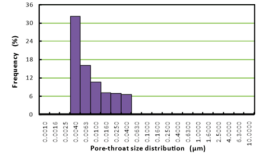
Reservoir type	1	2	3	4
Samples	Y432	B40,Y416,Y293	L330,Y438,Y414	Y299,L320
Reservoir physical properties	High	Medium	Low	Ultra low
Fractal dimension	$D_f=2.122$	$2.439 < D_f < 2.601$	$2.644 < D_f < 2.815$	$D_f > 2.776$
Pore types	Primary intergranular pore Residual intergranular pore	Residual intergranular pore Intragranular dissolution pore	Intercrystalline micropore Intragranular dissolution pore	Intercrystalline micropore
Microscopic characteristic				
Mercury intrusion and extrusion curves				
Pore-throat size distribution				

Fig. 11 Typical characteristics of four types of tight sandstone reservoirs

structures with large pore-throat sizes, poor reservoir permeability, intense diagenesis, and more pores with irregular shapes (Fig. 11).

Samples Y299 and L320 of type 4 have the lowest reservoir physical properties among the four types. The porosity is between 1.38 and 2.54% with a mean of 1.96%, and the permeability is between 0.003 and 0.006 mD with a mean of 0.005 mD. Type 4 has only one fractal dimension with a mean value of 2.862, which is closer to 3.0. This result indicates that the pore structures with the large and small pore-throat sizes are similar and that the fractal dimensions are the same. The casting thin sections show that samples of type 4 are very dense, with a large amount of clay mineral matrix filling between the clastic grains (Fig. 10e). The most prominent feature of type 4 samples is extremely strong compaction, which is the main reason for the loss of pore space and poor reservoir physical properties, while cementation and dissolution are not developed. In addition, because of the strong compaction, the

volume of intergranular pores decreases greatly or even disappears, and the intercrystalline micropores with a strong heterogeneity in the clay minerals become the main pore type (Fig. 10f). Therefore, samples with only one high fractal dimension reflect that the tight sandstone reservoirs have complex pore structures, the worst reservoir permeability, strong compaction, and fewer intergranular pores with regular shapes (Fig. 11).

The pore structures, including the pore-throat size, shape, and connectivity, are the most important factors in evaluating the reservoir quality in tight sandstone reservoirs. As mentioned above, fractal dimensions can reflect and assess the heterogeneity of pore structures in tight sandstone reservoirs. The samples with the two lowest fractal dimensions reflect that the reservoirs have better pore structures, higher reservoir permeability, weak compaction and cementation, and more pores with regular shapes. The samples with the highest fractal dimensions of large pore-throat sizes but low fractal

dimensions of small pore-throat sizes reflect that the reservoirs have complex pore structures with large pore-throat sizes, poor reservoir permeability, intense diagenesis, and more pores with irregular shapes. The samples with only one high fractal dimension reflect that the tight sandstone reservoirs have the most complex pore structures, the worst reservoir permeability, strong compaction, and almost no intergranular pores with regular shapes. In summary, fractal dimensions can be used as an effective parameter for the quantitative characterization of tight sandstone reservoirs with ultra-low permeability.

## Conclusions

The pore structures of tight sandstone reservoirs in the study area are complex and heterogeneous. Based on the shape of mercury injection curves, referring to reservoir physical property data and mercury injection parameters, the pore structures of 9 tight sandstone samples are divided into four types, which represent four different types of reservoirs. The fractal dimensions calculated by the mercury saturation method should be chosen to characterize the pore structures in tight sandstone reservoirs. There are clear turning points on the fractal curves in most samples, resulting from the fact that pore structures with large pore-throat sizes and small pore-throat sizes are relatively independent in tight sandstone reservoirs, and samples with different fractal characteristics represent reservoirs with different physical properties and pore structures. The samples with two low fractal dimensions represent the best reservoir, which reflects reservoirs that have better pore structures, higher reservoir permeability, weak compaction and cementation, and more pores with regular shapes. The samples with high fractal dimensions of large pore-throat sizes but low fractal dimensions of small pore-throat sizes represent the moderate reservoirs, which reflects the reservoirs that have complex pore structures in large pore-throat sizes, poor reservoir permeability, intense diagenesis and more pores with irregular shapes. The samples with only one high fractal dimension represent the worst reservoirs, which reflects that the tight sandstone reservoirs have the most complex pore structures, the worst reservoir permeability, strong compaction and almost no intergranular pores with regular shapes. In summary, fractal dimensions can be used as an effective parameter for the quantitative characterization of tight sandstone reservoirs with ultra-low permeability.

**Acknowledgments** The authors would like to thank PetroChina Changqing Oilfield Company for providing samples and data access.

**Funding** This study was financially supported by the National Major Science and Technology Projects of China (No. 2017ZX05009001 and No. 2017ZX05013-004-002).

## References

- Avnir D, Farin D, Pfeifer P (1984) Molecular fractal surfaces. *Nature* 308(5956):261–263
- Bustin RM, Bustin AMM, Cui A, Ross D, Pathi M (2008) Impact of Shale Properties on Pore Structure and Storage Characteristics. *SPE*. <https://doi.org/10.2118/119892-MS>
- Camp WK (2011) Pore-throat sizes in sandstones, tight sandstones, and shales: Discussion. *AAPG Bull* 95:1443–1444
- Cao L, Sun W, Sheng J, Huo L, Chen Q, Xie C (2016) A method to determine movable fluids saturation of low-permeability and tight oil reservoirs-by taking tight oil reservoirs in sixth member of Yanchang formation in banqiao area as an example. *J South Yangtze Univ (Natural Science Edition)* 13(20):1–8
- Chen C, Sun YM (1996) Fractional dimension of the pore-texture in sandstones and its application. *Acta Sedimentol Sin* 14(4):108–113
- Friesen WI, Mikula RJ (1987) Fractal dimensions of coal particles. *J Colloid Interface Sci* 120(87):263–271
- Gao H, Xie W, Yang JP, Zhang C, Sun W (2011) Pore throat characteristics of extra-ultralow permeability sandstone reservoir based on constant-rate mercury penetration technique. *Pet Geol Exp* 33(206-211):214
- Gao H, Yu B, Duan Y, Fang Q (2014) Fractal analysis of dimensionless capillary pressure function. *Int J Heat Mass Transf* 69:26–33
- Giri A, Tarafdar S, Gouze P, Dutta T (2012) Fractal pore structure of sedimentary rocks: simulation in 2-D using a relaxed bidisperse ballistic deposition model. *J Appl Geophys* 87:40–45
- He CZ, Hua MQ (1998) Fractal geometry description of reservoir pore structure. *Oil Gas Geol* 19(1):17–23
- Hu Q, Ewing RP, Dultz S (2012) Low pore connectivity in natural rock. *J Contam Hydrol* 133:76–83
- Ji W, Song Y, Jiang Z, Meng M, Liu Q, Chen L, Wang P, Gao F, Huang H (2016) Fractal characteristics of nano-pores in the Lower Silurian Longmaxi shales from the Upper Yangtze Platform, south China. *Mar Pet Geol* 78:88–98
- Jouini MS, Vega S, Mokhtar EA (2011) Multiscale characterization of pore spaces using multifractals analysis of scanning electronic microscopy images of carbonates. *Nonlinear Process. Geophys.* 18(6): 941–953
- Katz AJ, Thompson AH (1985) Fractal sandstone pores: implications for conductivity and pore formation. *Phys Rev Lett* 54(12):1325–1328
- Krohn CE (1988) Fractal measurements of sandstones, shales, and carbonates. *J Geophys Res Solid Earth* 93(B4):3297–3305
- Kulesza S, Bramowicz M (2014) A comparative study of correlation methods for determination of fractal parameters in surface characterization. *Appl Surf Sci* 293:196–201
- Lai J, Wang GW (2015) Fractal analysis of tight gas sandstones using high-pressure mercury intrusion techniques. *J Nat Gas Sci Eng* 24: 185–196
- Li K (2010) Analytical derivation of Brooks-Corey type capillary pressure models using fractal geometry and evaluation of rock heterogeneity. *J Pet Sci Eng* 73:20–26
- Li K, Home RN (2004) Universal capillary pressure and relative permeability model from fractal characterization of rock. In: *Th Stanford Geothermal Workshop on Geothermal Reservoir Engineering*. Stanford University, Stanford, California
- Li P, Sun W, Wu BL, Gao YL, Du K (2018a) Occurrence characteristics and influential factors of movable fluids in pores with different structures of Chang 6<sub>3</sub> reservoir, Huaqing Oilfield, Ordos Basin, China. *Mar Pet Geol*. 97:480–492
- Li Z, Wu SH, Xia DL, He SC, Zhang XF (2018b) An investigation into pore structure and petrophysical property in tight sandstones: A case of the Yanchang Formation in the southern Ordos Basin, China. *Mar Pet Geol* 97:390–406

- Liu Z, Zhu X, Liao J (2013) Sequence stratigraphy and genesis of sand bodies of the upper Triassic Yanchang formation in the southwestern margin of Ordos Basin. *Earth Sci Front* 20(2):001–009
- Mandelbrot BB (1977) *Fractals: Form, Chance, and Dimensions*. W. H. Freeman and Company, San Francisco
- Mandelbrot BB, Wheeler JA (1983) The fractal geometry of nature. *Q Rev Biol* 147:468
- National Development and Reform Commission, China (NDRCC) (2005) SY/T5346-2005: Rock Capillary Pressure Measurement.
- National Development and Reform Commission, China (NDRCC) (2006) SY/T5336-2006: Practices for core analysis.
- Pfeifer P, Avnir D (1983) Chemistry nonintegral dimensions between two and three. *J Chem Phys* 79(7):3369–3558
- Ross DJK, Bustin RM (2009) The importance of shale composition and pore structure upon gas storage potential of shale gas reservoirs. *Mar Pet Geol* 26:916–927
- Thompson AH, Katz AJ, Krohn CE (1987) The micro-geometry and transport properties of sedimentary rock. *Adv Phys* 36(5):625–694
- Wang HW, Anovitz LM, Burg A, Cole DR, Allard LF, Jackson AJ, Stacka AG, Rothera G (2013) Multi-scale characterization of pore evolution in a combustion metamorphic complex, Hatrurim basin, Israel: combining (ultra) small-angle neutron scattering and image analysis. *Geochim Cosmochim Acta* 121:339–362
- Wang M, Xue H, Tian S, Wilkins RWT, Wang Z (2015) Fractal characteristics of Upper Cretaceous lacustrine shale from the Songliao Basin, NE China. *Mar Pet Geol* 67:144–153
- Wu H, Guo YH, Zhang CL, Liu RE (2013) Characteristics and classifications of pore structure in tight oil reservoir: A case study of the Triassic Yanchang formation Chang7 in Longdong area, Ordos basin. *J Northeast Pet Univ* 37:12–17
- Xie S, Cheng Q, Ling Q, Li B, Bao Z, Fan P (2010) Fractal and multifractal analysis of carbonate pore-scale digital images of petroleum reservoirs. *Mar Pet Geol* 27:476–485
- Yang YT, Li W, Ma L (2005) Tectonic and stratigraphic controls of hydrocarbon systems in the Ordos basin: a multicycle cratonic basin in central China. *AAPG Bull* 89:255–269
- Yang H, Dou WT, Liu XY, Zhang CL (2010) Analysis on sedimentary facies of Member 7 in Yanchang Formation of Triassic in Ordos Basin. *Acta Sedimentol Sin* 28(2):254–263
- Yang H, Li SX, Liu XY (2013) Characteristics and resource prospects of tight oil and shale oil and shale oil in Ordos Basin. *Acta Pet Sin* 34: 1–11
- Zheng RC, Wang CY, Li H, Lei GM, Xie CH (2007) Provenance analysis of Chang 6 oil-bearing formation of Baibao-Huachi region in Ordos Basin. *Lithologic Reservoirs* 01:32–38
- Zhou Y, Ji YL, Xu LM, Che SQ, Niu XB, Wan L, Zhou YQ, Li ZC, You Y (2016) Controls on reservoir heterogeneity of tight sand oil reservoirs in Upper Triassic Yanchang Formation in Longdong Area, southwest Ordos Basin, China: Implications for reservoir quality prediction and oil accumulation. *Mar Pet Geol* 78:110–135
- Zhu RK, Wu ST, Su L, Cui JW, Mao ZG, Zhang XX (2016) Problems and future works of porous texture characterization of tight reservoirs in China. *Acta Pet Sin* 37:1323–1336
- Zhu YX, Sun W, Yu F (2008) Application of high-pressure Hg injection and rate-controlled Hg penetration experimental technique to studying reservoir microscopic pore structure: Taking Toutunhe Formation in Niuquanhu area of Santanghu oil-field as an example. *Nat Gas Geosci* 19:553–556
- Zou CN, Zhu RK, Liu KY, Su L, Bai B, Zhang XX, Yuan XJ, Wang JH (2012) Tight gas sandstone reservoirs in China: characteristics and recognition criteria. *J Pet Sci Eng* 88-89:82–91